Australian Journal of Basic and Applied Sciences, 5(10): 672-684, 2011
ISSN 1991-8178

Perforated Steel Shear Walls With Frp Reinforcement Of Opening Edges

Mohamad Alipour Tabrizi, Alireza Rahai

Department of Civil Engineering, Amirkabir University of Technology (Tehran Polytechnic), Tehran, Iran.

Abstract: Steel shear wall is an efficient lateral force resisting system with a thin steel plate connected to adjacent beams and columns which is expected to buckle in shear and form an inclined tension field similar to slender web plate girders. Sometimes the plate blocks a necessary building functionality and an opening is needed inside the plate. Examples of such cases are windows or doors in a steel shear wall core or openings for passage of ducts. The AISC seismic provisions states that an opening should be strengthened at edges by steel stiffeners to neutralize disruption of tension field continuity and minimize stress concentrations and edge buckling. It also allows other forms of openings that can be justified by testing or analysis. This paper introduces a method to prevent behavior decline using FRP laminates as edge reinforcement for the plate. An extensive numerical program was conducted to study the effect of FRP strips on the load carrying behavior of the system. A number of FRP materials together with different strip geometries are incorporated in the model to investigate possible behavioral improvements. The FRP layer is shown to prevent stress concentration at the perforation corners, provide support and continuity for inclined tension filed and enhance stiffness and strength of the shear wall system. The system is deemed to be promising considering the difficulties of traditional steel stiffeners which typically require welding and thus the proposed system can be equally efficient regarding economical and constructional considerations.

Key words: Steel plate shear wall, Perforation, FRP, Stress Concentration, Buckling.

INTRODUCTION

1.1. Perforated Steel Plate Shear Walls :

Steel plate shear wall (SPSW) is a lateral resistant system in which a thin steel plate is attached at top and bottom edges to two consecutive beams and at side edges to two columns in a span. The plate undergoes shear buckling and then a post-buckling phenomenon similar to that of inclined tension field in a plate girder occurs which is dependent on stiff and strong boundary frame elements. In some situations it may be necessary to cut the plate to place windows, doors or other openings which may undermine post-buckling behavior by weakening interior boundaries of the plate adjacent to the opening. The area around the perforation does not have a support at one side and therefore it is not able to develop inclined tension field and ultimately yield in tension.

The current practice for such perforated shear walls is to attach local boundary elements (or stiffeners) such as steel channels, angles or I sections to the four sides of the perforation so as to provide support for the inclined tension field and transfer plate edge loads at sides of perforation to the plate and perimeter boundary elements (AISC, 2005; AISC, 2007). Such an approach is depicted in figure 1.

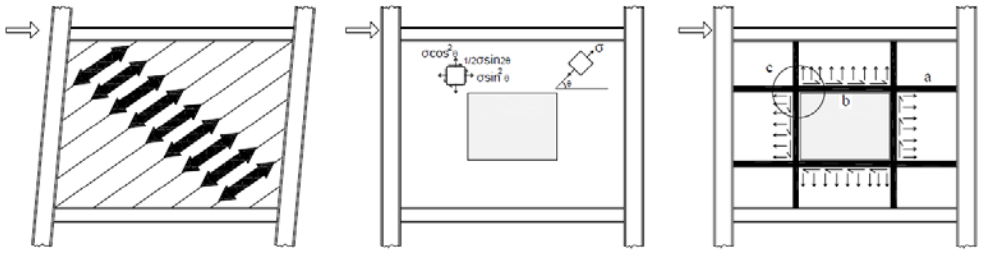

Fig. 1: Inclined tension field in SPSW infill (left), Principal stresses in plate (center) and forces acting on perforation boundary elements (right)

The AISC seismic provisions for steel buildings (AISC, 2005) states that "Openings in webs shall be bounded on all sides by HBE and VBE extending the full width and height of the panel respectively, unless otherwise justified by testing and analysis". Furthermore, AISC design guide 20 provides a discussion on design

Corresponding Author: Mohamad Alipour Tabrizi, Department of Civil Engineering, Amirkabir University of Technology (Tehran Polytechnic), Tehran, Iran.
E-mail: mohamadealipour@yahoo.com

of perforated steel shear walls where steel boundary elements are analyzed and designed for inclined yielding stresses of the adjacent plate (AISC, 2007).

1.2. FRP Stabilization and Strengthening of Thin-Walled Steel Sections:

Strengthening thin-walled steel structures has attracted increasing attention and different issues have been studied in the past decade (Zhao and Zhang, 2007). Extensive research has been focused on such areas as tension flange strengthening of beams (Tavakkolizadeh and Saadatmanesh, 2003; Photiou, *et al.*, 2006), jacketing steel tubes and cylinders (Teng and Hu, 2007; Bambach, *et al*., 2009), FRP-steel adhesive bond behavior (Xia and Teng, 2005; El Damatty and Abushagur, 2003) and buckling control in slender box columns (Shaat and Fam, 2006). A part of past research has addressed buckling mitigation and plastic hinge stabilization by restraining free edge deformations.

Accord and Earls investigated the effect of 6.4mm thick GFRP strips attached to compression flange edges of a cantilever steel beam (Accord and Earls, 2006). They did not include FRP fracture or debonding in analysis and concluded that the FRP strip enhanced section ductility by restraining free edge deformations and buckling control by imposing a nodal line on the plate elements.

(Harries, *et al*., 2009) conducted an experimental study wherein steel sections were partially stabilized using narrow FRP strips (Harries, *et al.*, 2009). They stated that the high stiffness and linear behavior of FRP materials are utilized to provide ‘‘bracing’’ against web or flange local buckling. Cyclic concentric compression tests of long and stub WT sections (perhaps as in steel bracings) were carried out to study probable effects of FRP on elastic and plastic buckling of the section. They reported insignificant effect of FRP on ultimate axial capacity but observed an effective delay in buckling and a decrease in lateral deformations associated with buckling.

1.3. FRP-Composited Steel Plate Shear Walls:

Although steel plate shear walls are proved to have acceptable behavior, a number of issues emerge. Plate instabilities restrain energy dissipation of the system which is demonstrated as pinching of the hysteresis curves. A thick or stiffened plate will yield in shear which is a more ductile behavior and increases energy dissipation. On the other hand, buckling-induced out-of-plane deformations of the plate may cause nonstructural damage. The inclined tension field also exerts strong inward forces on beams and columns compared with a plate which yields in shear before buckling happens. To address these issues Astaneh-Asl proposed a composite system wherein reinforced concrete layers were connected to the thin plate using studs. The RC layer would act as lateral support and facilitate shear yielding by mitigating buckling (Astaneh-Asl, 2002).

In a series of cyclic tests on SPSWs, Hatami and Rahai tested three one-storey SPSW models with 3 mm thick steel plate and 2IPE200 beams and columns. In one of the models, the steel infill plate was composited by attaching a 0.176mm thick CFRP layer using epoxy resin. Comparing the acquired data, the researchers observed less damage in the retrofitted specimen along with rupture of some bolts connecting the plate to the boundary members. They also found the FRP layer responsible for 37% increase in energy dissipation and 50% in lateral stiffness. It was stated however that FRP bonding had decreased ductility of wall by 8% (Hatami and Rahai, 2008).

Alipour carried out a numerical investigation on buckling and post-buckling behavior of FRP-composited steel shear walls after a vast literature survey on FRP-steel rehabilitation systems and bond behavior. A steel infill plate under pure shear was studied for buckling using elastic eigen-value analysis and its post-buckling phase was simulated using plasticity for steel and progressive damage for FRP materials. Both the buckling and post-buckling analyses demonstrated the ability of FRP layer to act as elastic support for the thin steel plate and hence a significant increase in buckling capacity, control of plastic flow in steel, decrease in out of plane deformations and increase in lateral stiffness and strength of the SPSW system (Alipour, 2010).

Rahai and Alipour investigated the fiber direction and geometry for FRP-composited steel shear walls using the finite element method. It was found that the optimum direction for fibers is the direction of tension field in the plate as can be calculated using an energy-based formula (Rahai and Alipour, 2011).

The idea of using FRP as edge reinforcement for perorated SPSWs was first proposed by Alipour and Raeeszadeh (Alipour and Raeeszadeh, 2011). Horizontal and vertical FRP strips used as edge stiffeners proved the proposed method as a valuable alternative to steel stiffeners.

1.4. Concept and Research Significance:

The concept of FRP stabilization of steel members has considerable background in literature. In this study, FRP strips have been attached to perforation edges to stabilize and stiffen plate edges and to provide support for establishment of tension field around the opening. This paper studies effectiveness of FRP strips as perforation boundary elements and the effect of FRP strip thickness, width and material type on wall behavior.

To authors’ knowledge, this paper presents the first research on FRP-stiffened perforated SPSWs. However, the idea is thought to be especially interesting to researchers considering the following advantages. First, FRP bonding is much easier and faster than steel stiffener welding specially with regard to difficulties of welding

very thin steel plates. In addition, the idea can be applied to other applications where a perforated steel plate under shear needs stiffening such as openings in slender plate girder webs.

MATERIALS AND METHODS

2.1. Model Properties:

The steel plate shear wall model was designed using the guidelines outlined in AISC seismic provisions. According to AISC 341-05, the design of a steel plate shear wall is considered acceptable when the plate undergoes considerable yielding prior to yielding in the boundary members. Moreover, with the increase in storey drift, yielding must occur in the ends of the HBEs so as to ensure a safe load path for the gravity loads. The centerline height and width of the frame are 3000 mm and a 3 mm steel plate is used. The yield force of the infill plate was applied on the beams and columns at the angle of tension field and the boundary frame members were designed accordingly. Reduced beam section connections were used to reduce the beam plastic moment on the column ends. The designed SPSW details together with its yield pattern at 2.5% drift are illustrated in figure2. The yield pattern confirms that the design complies with AISC 341-05.

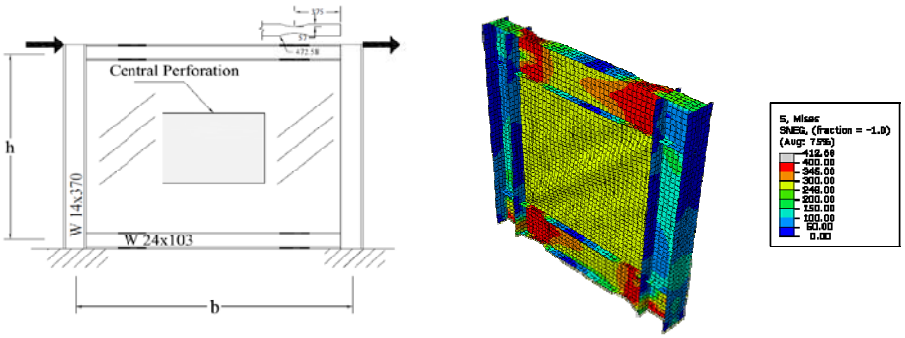

Fig. 2: Designed model details (left) yield pattern at 2.5% drift (right).

ASTM A36 and ASTM A572 Gr.50 steel were used for the infill plate and the boundary frame members respectively. In order for the infill plate to yield earlier than the frame members, steel with lower yield stress (A36) was used for the infill plate. Elastic perfectly plastic stress-strain curves with F_y=248 MPa and E=200 GPa and ν=0.3 for the elastic range were used.

2.2. Finite Element Procedures:

Modeling and analysis of the SPSW models were carried out using the ABAQUS finite element package (ABAQUS, 2008). Models were simulated using 2-dimensional shell parts and the four-noded reduced integration S4R shell elements were used in meshing. First, an eigen-value buckling analysis was performed on the models to acquire the buckling shapes of the model and the first buckling mode shape was introduced to the models so as to account for the initial imperfections of the plate. The mode shapes were scaled to produce a largest out-of-plane deformation equal to the plate thickness. Geometric and material nonlinearity effects were accounted for and the overall modeling procedure was carefully verified by simulation of two large-scale experiments available in the literature.

Behavior of FRP materials is modeled through elastic behavior, damage initiation and damage evolution models incorporated in ABAQUS software (ABAQUS, 2008). Orthotropic elastic behavior is defined through introduction of elastic coefficients (E_{11}, E_{22}, G_{12}, ν_{12}) in a local coordinate system with the main 1-direction along the fibers. Initiation of damage at a specific point is examined through calculation of Hashin failure criteria and once a criterion is met in a longitudinal, transverse or shear mode, corresponding stiffness will be reduced according to a linear softening rule. Tensile and compressive strength in the fibers (X^T, X^C) and matrix direction (Y^T, Y^C) and shear strength (S) are experimentally evaluated by testing standard material coupons and are used to predict failure initiation. The softening rule governing damage evolution in each failure mode is based on the energy dissipated during fracture.

Four different FRP materials were carefully selected from the wide range of materials whose mechanical properties were previously reported in the literature through testing so as to represent different possible mechanical properties. Table 1 shows the mechanical properties of the FRP materials used in the analysis. In some cases where specific data (especially fracture energies) were not reported, the data were assumed based on comparison with similar cases.

Table1: Mechanical properties of the selected FRP materials

Material	E_{11} (GPa)	E_{22} (GPa)	G_{12} (GPa)	V_{12} -	X^T MPa	X^C MPa	Y^T MPa	Y^C MPa	S MPa	$G_{f,t}$ N/mm	$G_{f,c}$ N/mm	$G_{m,t}$ N/mm	$G_{m,c}$ N/mm
CFRP	146.8	11.4	6.1	0.3	1730	1379	66.5	268.2	58.7	89.83	78.27	0.23	0.46
HM-CFRP	450	11.4	6.1	0.3	1540	1232	66.5	268.2	58.7	100	100	0.23	0.46
HS-CFRP	210	11.4	6.1	0.3	3200	2560	66.5	268.2	58.7	100	100	0.23	0.46
GFRP	20.3	11.4	6.1	0.3	855	684	66.5	268.2	58.7	12.5	12.5	0.23	0.46

2.3. Validation:

2.3.1. Steel Plate Shear Wall Behavior :

To verify modeling of a SPSW and nonlinearity and post-buckling phenomenon in its behavior, two examples of famous laboratory tests were selected and simulated using the ABAQUS finite element package. The first example is the four-storey shear wall tested in the University of Alberta (Driver, *et al*., 1997). S4R shell elements with material and geometric nonlinearity were used and an imperfection following the first buckling mode of the system was applied to the model with maximum deflection of 20 mm to simulate the real imperfect conditions. Shear force of the first storey was monitored and plotted against first storey in-plane displacement and comparison of the FE pushover curve with the laboratory hysteresis curves is shown in figure3.

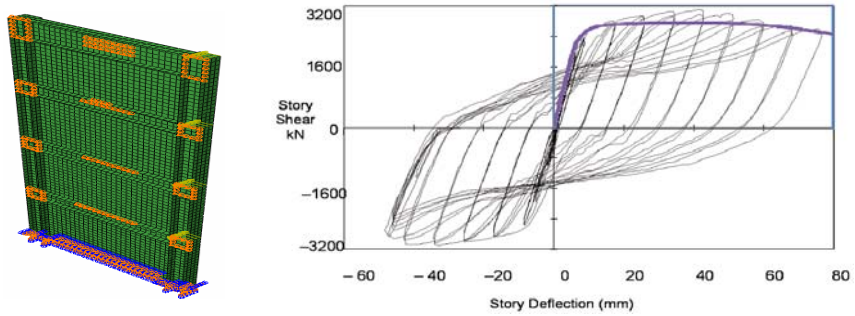

Fig. 3: Verification of Alberta model.

The second example is the one-story perforated shear wall recently tested in Taiwan by the researchers of the University of Buffalo (Vian, *et al.*, 2009). Perfect agreement between the FE results gained in this verification and both the FE and experimental results reported by (Vian, *et al*., 2009) is demonstrated in figure 4.

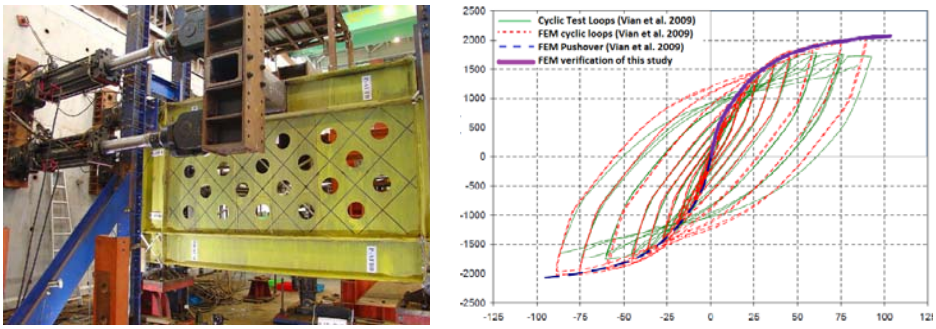

Fig. 4: Verification of Vian, *et al*. model (Vian, *et al.*, 2009).

The good agreement achieved in both examples may demonstrate the ability of the adopted procedures to simulate key features of a SPSW behavior.

2.3.2. FRP-Steel Composite Action and Inclusion of Damage and Plasticity:

Interaction of metal plasticity and FRP fracture and damage behaviors is an important part of the current study. To investigate the ability of the finite element procedures used in this study in predicting such phenomena, a fiber metal laminate (FML) specimen found in the literature was modeled and analyzed. The FLM consisted of three thin aluminum layers bonded with two GFRP layers under tension with a central hole as depicted in figure 5. This problem was modeled using solid elements for the aluminum and GFRP layers and cohesive elements for the adhesive films by Lapczyk and Hurtado and they compared their analytical results with experimental FML strength and observed considerable agreement (Lapczyk and Hurtado, 2007). However, in the current study S4R shell elements were used and perfect bond was assumed between layers. Comparison of the force-displacement curve obtained by Lapczyk and Hurtado and that of this study in figure 6 shows very good agreement.

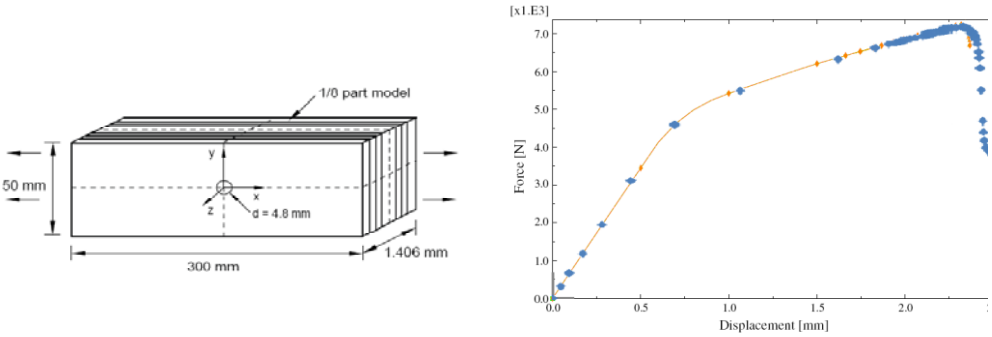

Fig. 5: Validation of composite behavior (Lapczyk and Hurtado, 2007).

In this study, a strong adhesive system with additional measures to mitigate debonding is assumed so as to validate perfect adhesion assumption for the purpose of current study. To authors' knowledge, the same attitude is selected in most of past studies aimed at FRP-stabilization of steel researches.

2.3.3. Mesh Sensitivity Analysis:

In order to investigate the effect of discretization on the numerical results, the shear walls model introduced in figure 2 was pushed and analyzed without a perforation and the analyses were repeated for different mesh sizes. The difference of base shear and initial stiffness of the wall with those of the smallest mesh for each mesh size are plotted against the number of elements in figure 6. Both of the error curves show convergence and a mesh size of 75 mm was adopted for the model corresponding to 2.3% and 0.6% error for base shear and stiffness respectively.

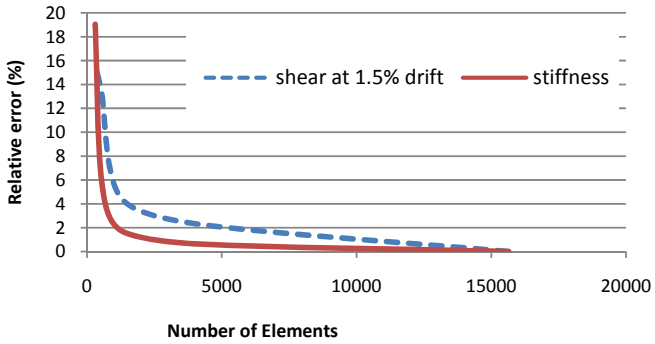

Fig. 6: FE mesh convergence analysis.

As a second mesh sensitivity analysis, the steel infill plate of the model in figure 2 with dimensions of 2500*2500*3mm was analyzed using elastic eigen-value procedure and the critical shear buckling stresses were extracted for different mesh sizes and the difference between FEM critical shear buckling stress results for different mesh sizes with that of exact analytical stress as given by equation 1 is plotted against number of elements (Figure 7). Based on figure 7, mesh size of 75mm which was used for the analyses in this section yields satisfactory results with less than 1% error from the exact answer.

$$\tau_{cr} = \frac{k\pi^2 E}{12(1-\vartheta^2)}\left(\frac{t}{b}\right)^2$$

$$k = 5.34 + \frac{4}{(\frac{a}{b})^2}$$

Equation 1

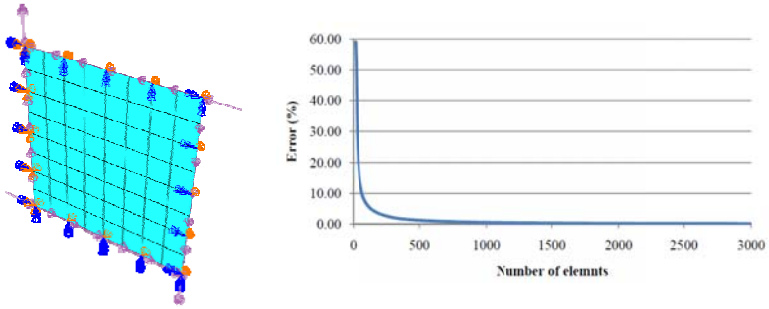

Fig. 7: Model for buckling stress mesh study and percentage errors from exact answer.

Numerical Investigations and Discussions:

4.1. Parameter Definitions:

For each model the load-displacement pushover curve is extracted. The curve is then idealized with a bilinear curve with equal initial slope and ultimate strength and a yield point is defined for each bilinear curve by equating the enclosed area under the real and the idealized curves as depicted in figure 8. Using the idealized curve, quantitative measurement of the behavior of the composite SPSW is done through strength parameters (F_u and F_y), lateral stiffness (K), area enclosed by the load-displacement curve (A). Therefore, for each model four parameters (F_u, F_y, K and A) are calculated.

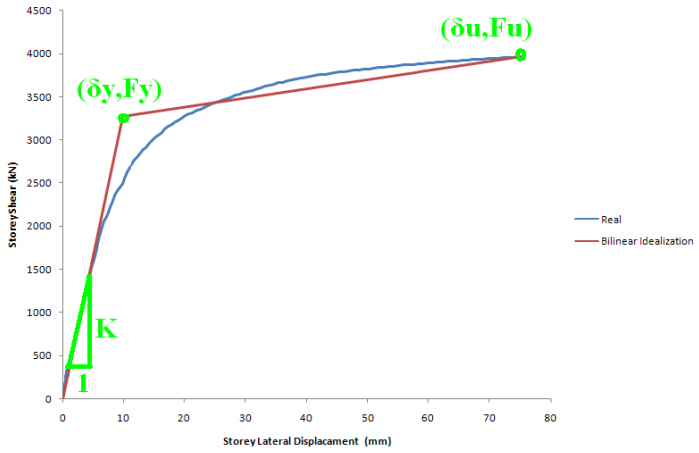

Fig. 8: Bilinear idealization of load displacement curves.

In order to gain a better understanding of the effect of FRP on characteristics of SPSW, a normalization scheme has been employed herein. Design of SPSW according to current regulations (AISC seismic provisions and AISC Design guide 20) necessitates the use of very strong boundary elements as there are strict limitations on their stiffness and strength. The plate must yield before any boundary element plastifies and plastic hinges are not permitted except at beam ends. These provisions have led to plate contributing to story shear less than the frame in the designs by researchers (Vian, *et al.*, 2009; a and b; AISC, 2005). Therefore, FRP strengthening effect will not be properly realized unless its contribution is normalized relative to contribution of the steel plate. For this purpose, shear and stiffness contribution of plate is calculated by deducting open frame shear and stiffness from those of SPSW (plate+frame). This simple deduction even in plastic range has been widely accepted and used by researchers. (Sabouri, *et al.*, 2005)named this approach plate-frame interaction (Sabouri, *et al.*, 2005) while Berman and Bruneau calculated plate-only hysteresis curves by deducting hysteresis curves of experimental open-frame from those of SPSW (Berman and Bruneau 2005).

In this paper, plate contribution to storey shear is calculated as:

equation 2

$$F_{u,p} = F_{u,SPSW} - F_{u,f}$$

And FRP contribution to storey shear is calculated as:

equation 3

$$F_{u,FRP} = F_{u,CPSW} - F_{u,SPSW}$$

Where;
$F_{u,SPSW}$= Total storey shear carried by SPSW
$F_{u,p}$= Contribution of plate in total storey shear
$F_{u,f}$= Contribution of frame in total storey shear
$F_{u,CPSW}$= Total storey shear carried by FRP-strengthened SPSW

The same deductions will be done for stiffness, yield shear and enclosed area and K_{FRP}, $F_{y,FRP}$ and $A_{,FRP}$ denote FRP contribution to stiffness, yield shear and enclosed area respectively.

4.2. Effect of Perforation:

A typical central 1000 mm square perforation was made in the model and the shear and stiffness share of the plate is calculated using eq.(2) and summarized in table 2 for solid and perforated plate. Perforation is responsible for a substantial decrease in shear and stiffness.

Table 2: Effect of perforation on SPSW performance.

	Plate share in SPSW	perforated plate share	Effect of perforation (%)
K (kN/mm)	212.4	102.7	-51.6
F_u (kN)	736.8	250	-66.1
A (kN.mm)	55694.8	22428	-59.7
F_y (kN)	401.8	47.4	-88.2

Figure 9 shows principal strain and mises equivalent stress distributions and principal stress vector orientations in the infill plate of a solid-plate SPSW. The plate has yielded completely and a rather even strain distribution with maximum 5.4% strain and a uniform tension filed at an angle near 45° is visible. This figure and all the subsequent stress states are extracted at 2.5% lateral storey drift (as an arbitrary ultimate state) for comparison.

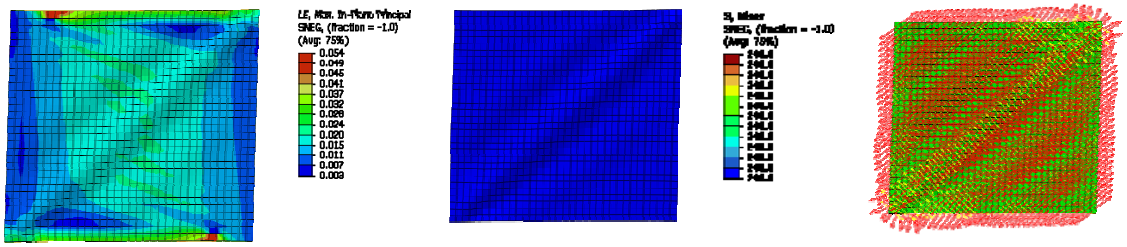

Fig. 9: Principal strain, mises stress and principal stress vector distributions in solid infil SPSW.

Figure 10 shows the infill plate with a 1000mm square opening with free edges. The strain plot shows an intense concentration at opening corners with 24.4% strain which is the result of simultaneous divergent shear and tension as was depicted in figure 1. The stress plot shows that the plate is not able to develop tension field while the vector plot shows a non-uniform stress field.

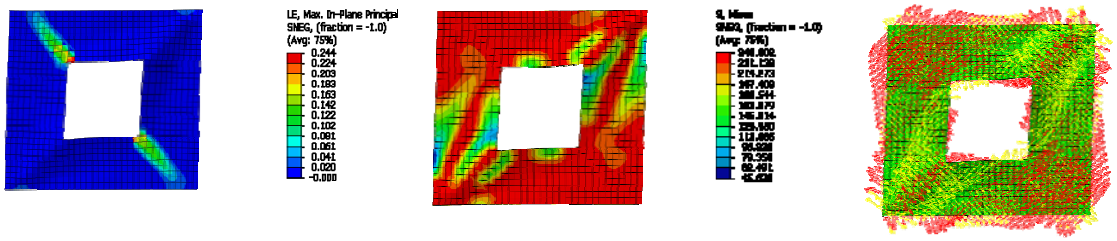

Fig. 10: Principal strain, mises stress and principal stress vector distributions in unreinforced perforated SPSW.

The effect of perforation size on SPSW lateral capacity can be realized in figures 11 and 12 where the perforation dimension is increased from zero (no perforation) to 2500 mm and the corresponding shear-displacement pushover curves are plotted for comparison. It can be seen that the perforation substantially decreases both stiffness (slope of the initial linear phase) and the ultimate shear strength of the wall.

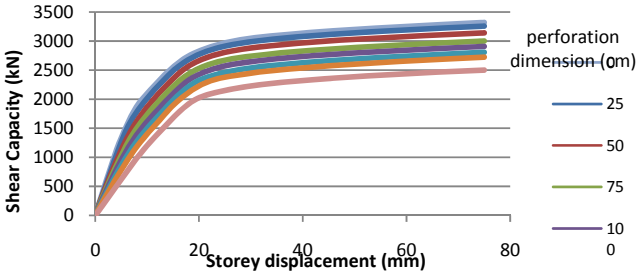

Fig. 11: Effect of perforation dimension on SPSW shear-displacement pushover curves.

Diagrams of figure 12 highlight a linear pattern in SPSW strength and stiffness decrease with increase in perforation size. It should be noted that a similar linear pattern was observed for perforated steel plate shear walls with a circular central perforation in tests conducted by Roberts and Sabouri-Ghomi and they commented that a similar pattern must exist in walls with square perforations (Roberts and Sabouri-ghomi, 1992).

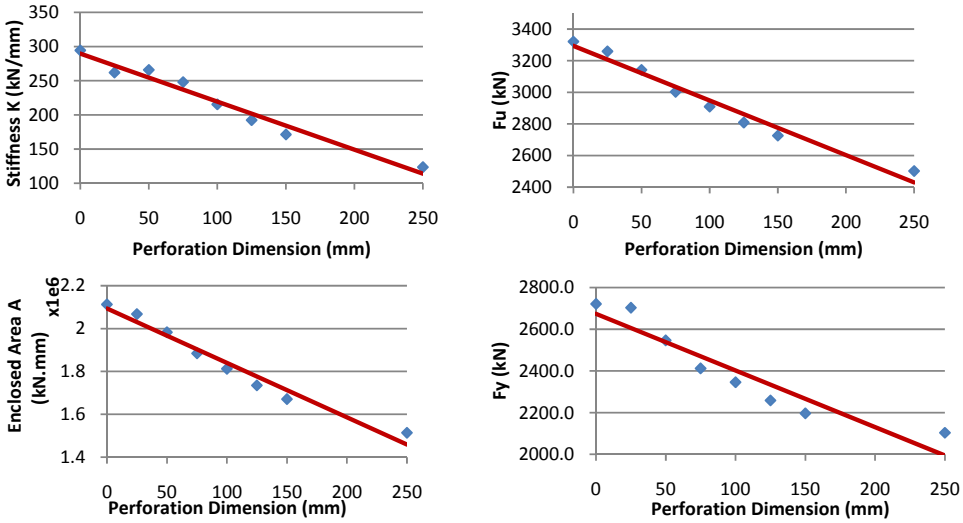

Fig. 12: Linear decrease of SPSW strength and stiffness with increase in perforation size.

Stress plots of figure13 demonstrate how perforation dimension exerts its adverse effect on the ability of the plate to undergo full yielding and therefore its ductile behavior and energy dissipation. In the plate with the largest perforation, plate yielding is entirely disturbed which is because there is no support at the perforation edge for the inclined tension which amplifies the stresses to yielding. This emphasizes the need for providing support of a suitable kind at the free perforation edges.

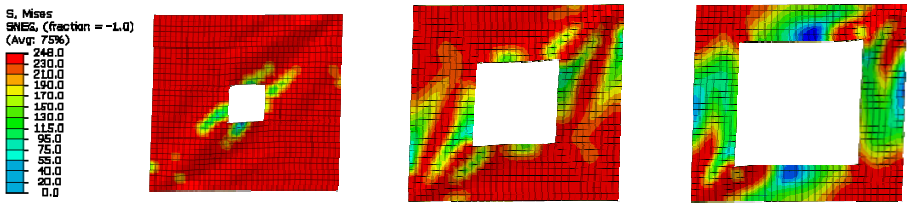

Fig. 13: Mises equivalent stress distribution for unstiffened walls with different perforations.

.3. Edge Stiffening Using FRP Strips:

CFRP strips of 100mm, 200mm and 300mm widths are attached to four edges of perforation as depicted in figure 14 and the corresponding contributions of FRP strips to stiffness, strength and enclosed area are calculated using eq.(3).

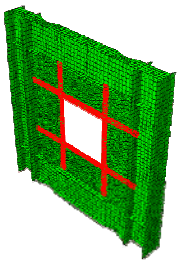

Fig. 14: Configuration of pattern A.

The percentage contribution of FRP compared to solid plate contribution is given in charts of figure 15. Note that stiffness, strength and area of the steel plate were decreased as a result of perforating by 51.6%, 66.1% and 59.7% respectively as earlier given in table2.

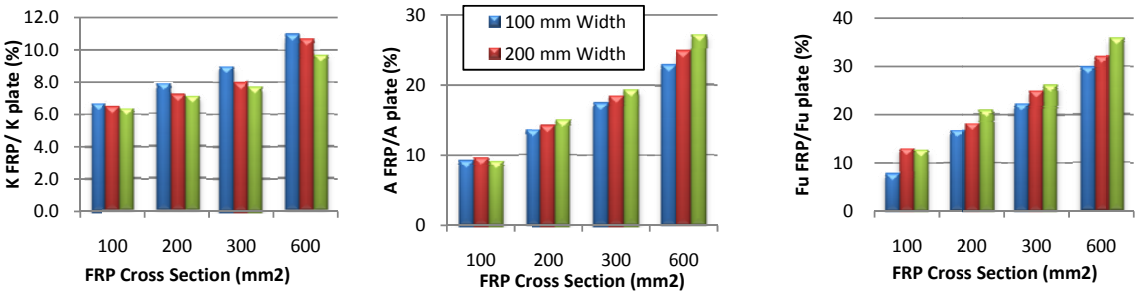

Fig. 15: Percentage FRP to Plate share in stiffness, capacity and area of different widths of FRP.

4.4. Effect of FRP Strip Width:

In order to investigate the effect of FRP width on the behavior of the system, diagrams of figure16 are presented. In these figures, considering a constant amount of FRP, say 500 mm^2 of cross section, stiffness of the wall is the highest for the narrowest FRP strip. In contrast, for that same amount of FRP, the ultimate strength (F_u), Yield strength (F_y) and Enclosed area (A) increase with increase in strip width.

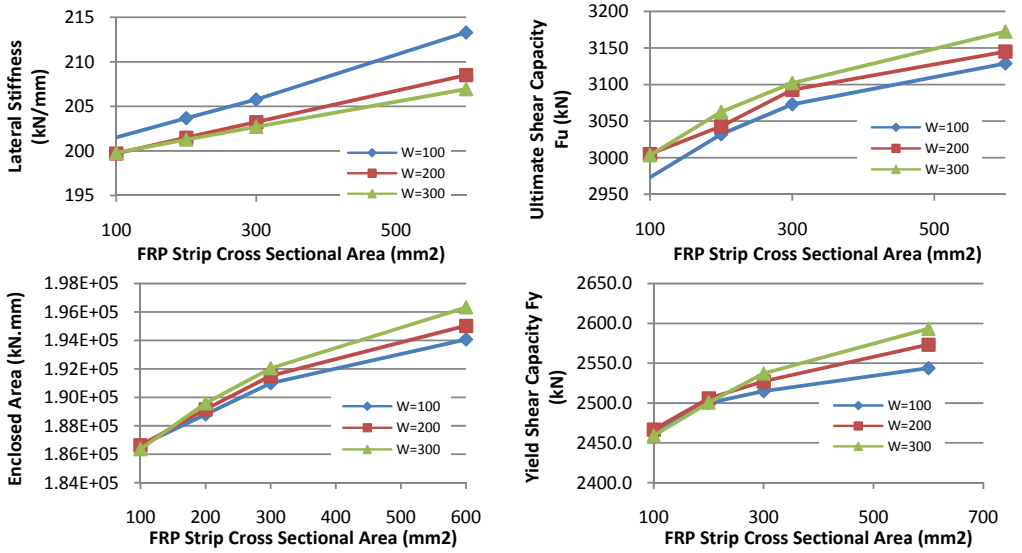

Fig. 16: Effect of width on SPSW behavior parameters.

To discuss the reasons for this behavior, a look at stress distribution plots of figure17 will be helpful. When the same FRP amount is spread to a larger width, better stress distribution is gained and therefore stress concentrations associated with sudden cut of the plate is allocated to a bigger width. This prevents intense local stress concentrations and localized plastification at perforation corners and thus the plate manages to employ larger area to tension field action. It is noted from figure17 that maximum principal strain at perforation corner decreases from 24.4% of unstiffened perforated SPSW of figure9 to 12% and 6.8% in 100mm and 300 mm wide FRP strips respectively. More uniform stress distribution and tension filed is obvious in the corresponding plots.

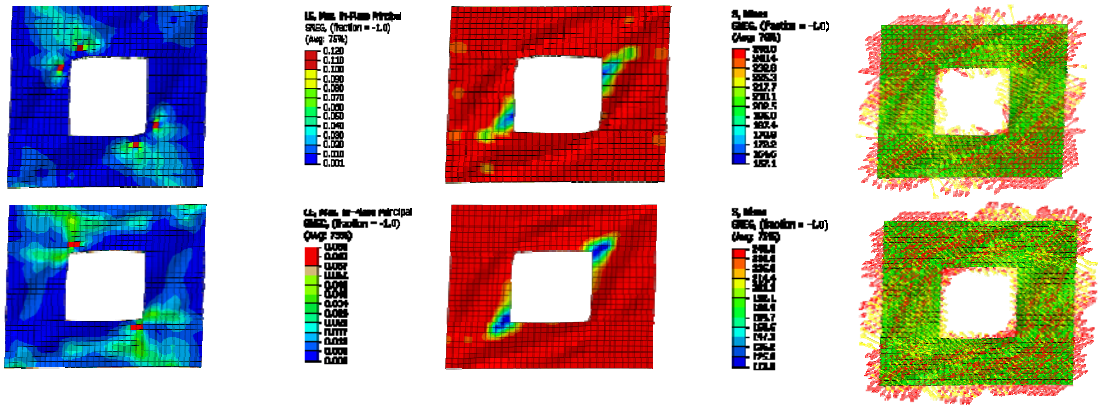

Fig. 17: Stress and strain distribution of models of FRP width 100mm (top row) and 300mm (bottom row).

In contrast, when discussing stiffness curves of figure16 one should remember that lateral stiffness is calculated as initial tangent of load-displacement curve or as is the case with this paper, slope of the point corresponding to 0.1% drift on that curve. This point was arbitrarily chosen as a point located on preliminary stages of fully linear behavior of the wall. Therefore, initial lateral stiffness has nothing to do with ultimate stress distribution nor does it involve any plastification. The reason for this is that such a strip will have more flexural resistance (i.e. bigger moment of inertia). The narrower strip will restrain out-of-plane deformations better, restrains buckling and keeps the steel plate straight and planar and therefore produces higher lateral stiffness.

4.5. Effect of FRP Material Type:

Mechanical properties of the FRP material employed in the strengthening may change effectiveness of the design. A comparison was made between four types of FRP materials of table 1 as edge reinforcement and presented in figure 18. The FRP strip in these models is 300mm wide and 3 mm thick. The figure shows that highest stiffness and strength are gained using the FRPs with highest modulus (HM-CFRP) and highest longitudinal tensile strength X^T (HS-CFRP) respectively. The material named CFRP which is a typical commercial carbon FRP gives reasonable results in terms of both stiffness and strength.

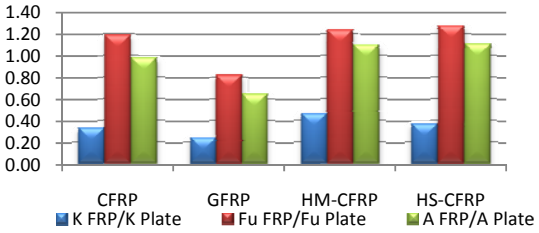

Fig. 18: Effect of FRP material type on SPSW behavior.

4.6. Diagonal FRP configuration:

In an effort to find a more efficient pattern for FRP strips, a closer look at the force transfer mechanism depicted in figure 1 can be useful. As was discussed previously, at two corners of the opening the tension and the divergent shear act in the same way to intensify the stress concentration and the resultant stresses will be along the diagonal of the opening at a 45º angle. Other than the horizontal and vertical strip configuration (pattern A) discussed above, FRP strips can be oriented in the direction of the resultant tensile stress. In other words, the fibers are oriented at the direction of maximum tension at an angle of 45º at corners of the opening as shown in figure 19(a).

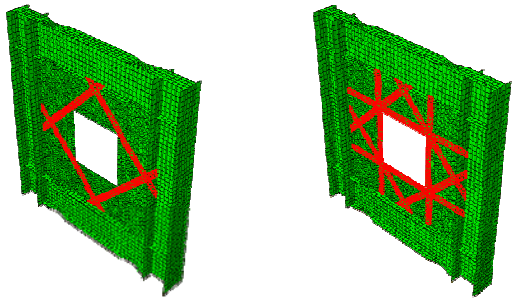

Fig. 19: (a) Configuration of pattern B, (b) pattern C.

Contours of figure 20 (left and center) show strain and stress distribution in pattern B at 2.5% drift. Maximum strain of 17.4% at corners shows that the corners are subject to heavily localized effects. The fiber tensile damage contour of figure 20 (right) shows that the FRP strips have not been strong enough to resist the inclined tension and have undergone tensile damage. Note that tensile damage factor (DAMAGEFT) equal to 1 shows complete FRP rupture.

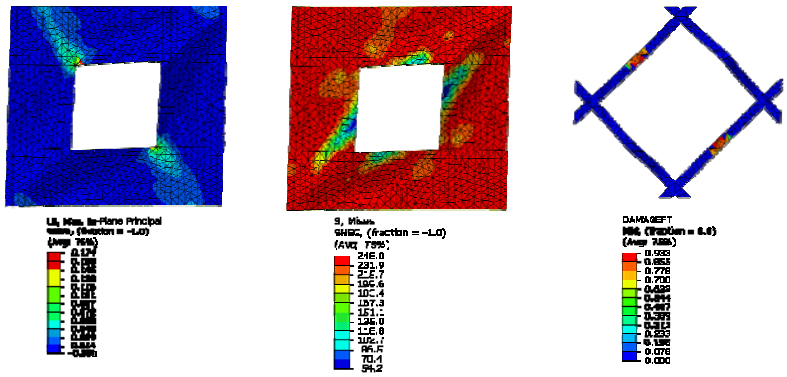

Fig. 20: Principal strain contour (left), principal stress (middle) and FRP damage factor (right).

Figure 21 shows pushover curves for the shear wall with and without perforation, the perforated wall strengthened with pattern A and the same model with pattern B. It is obvious that in pattern B in spite of the initial increase in stiffness and strength compared to pattern A, the curve experiences a sharp fall and finally lies back on the unreinforced curve. The sudden decline is obviously attributed to the onset of FRP damage. The fibers which are subject to maximum tension are damaged and ruptured as depicted in figure 20 right and the contribution of FRP strips suddenly vanishes afterwards.

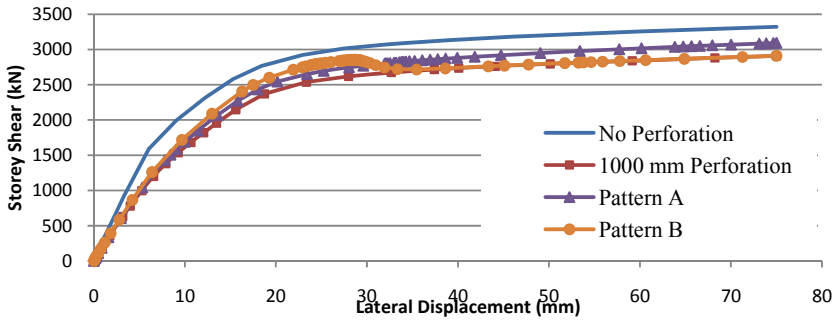

Fig. 21: Pushover curves of SPSW with and without perforation and with patterns A and B.

The last configuration tested here is a combination of patterns A and B denoted as pattern C as depicted in figure 19b. The stress and strain distributions corresponding to this pattern are presented in figure 22 and a comparison between parameters of patterns A and C is given in table 3. Figure23 shows that strain concentration is reduced compared with pattern A and a more uniform stress distribution demonstrates the ability of the FRP

system to allow overall plate yielding. Table 3 however highlights that pattern C may not be optimum because the parameters are not doubled while FRP volume is nearly doubled. A more detailed research program is needed to determine the optimum configuration as a compromise between increasing thickness and adding inclined FRP strips. It should be noted that pattern C may be more efficient against localized effects and debonding compared with pattern A with double thickness.

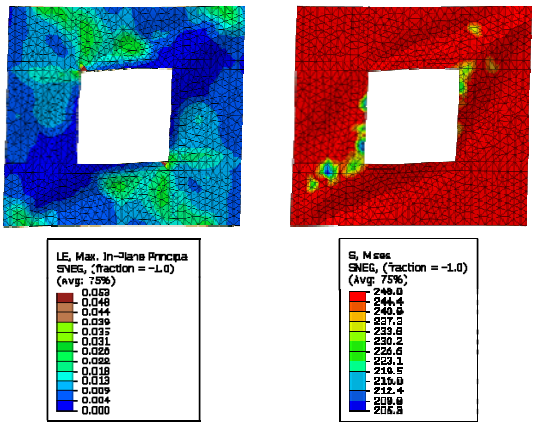

Fig. 22: Principal strain and stress contours in pattern C.

Table 3: Comparison of Parameters in patterns A and C

	Pattern A	Pattern C
K (% relative to plate)	16.2	19.8
Fu (% relative to plate)	40.4	76.3
A (% relative to plate)	39.6	63.8
Maximum strain (%)	12%	5.3%

4.7. Further Notes:

Due to high complexity of the present model incorporating steel plasticity, buckling instabilities and FRP fracture at the same time, introduction of debonding to this model was cumbersome at the moment. As such, a step by step approach is considered in which the general and global behavior of the system is to be studied fully in the first step (which is presented in this paper) and local complexities such as debonding is to be studied in a separate model with proper simplifications. At present, a strong adhesive system with additional measures to mitigate debonding is assumed so as to validate perfect adhesion assumption for the purpose of current study. To authors' knowledge, the same attitude is selected in most of past studies aimed at FRP-stabilization of steel researches. The significance of the present study however remains intact considering the outlook gained into thin steel plate buckling and post-buckling stabilization provided by the FRP layer as an elastic support.

Conclusions:

It may be necessary to place an opening in the infill plate of a steel plate shear wall. Severe buckling and lack of support for inclined tension field action at free edges undermine SPSW behavior. Therefore, FRP strips were used as edge reinforcement around opening in a perforated SPSW which can possibly be a faster and easier alternative to traditional steel stiffeners. The idea was studied through an extensive finite element study wherein the following results were obtained:

- The FRP stiffening is found to restrain strain concentrations, provide support for inclined tension struts and retrieve tension filed action of the plate.
- Strain concentration at perforation corners is decreased substantially by the use of FRP strips. The 24.4% principal strain at corner of unstiffned plate decreases to 12% and 6.8% for models with $100^{mm}*3^{mm}$ and $300^{mm}*1^{mm}$ CFRP strips respectively.
- The proposed FRP stiffeners of different widths compensate for 7-11% stiffness, 8-35% strength and 10-26% energy dissipation of the steel plate while the perforation decreases plate stiffness, strength and energy dissipation by 51%, 66% and 59% respectively.
- Lateral stiffness is maximized using narrower and thicker strips while strength and energy dissipation are maximized with wider and thinner strips. An explanation for this phenomenon is presented.
- The highest stiffness and strength are gained using the FRPs with highest modulus (HM-CFRP) and highest longitudinal tensile strength X^T (HS-CFRP) respectively.

- Inclined FRP strips oriented at 45º at opening corners may be another pattern for stiffening but may be subject to fiber rupture and sudden loss of strength as a result of maximum tensile forces at opening corners.

REFERENCES

ABAQUS/Standard Analysis User's manual, version 6.8-1, 2008. Hibbitt, Karlsson, Sorenson Inc, (HKS).

Accord, N.B. and C.J. Earls, 2006. Use Of Fiber Reinforced Polymer Composite Elements To Enhance Structural Steel Member Ductility, ASCE J Comp Constr, 10(4): 337-44.

AISC design guide 20, Steel Plate Shear Walls, 2007. American Institute of Steel Constr., Chicago, IL.

AISC Seismic Provisions for Steel Buildings, 2005. American Institute of Steel Constr.,Chicago, IL.

Alipour Tabrizi, M., 2010. Evaluation of the effect of FRP layer characteristics on SPSW behavior, MSc dissertation, Dept. civil eng., Amirkabir University of Technology, Tehran, Iran.

Alipour Tabrizi, M. and A. Raeeszadeh, 2011. Introduction of an Innovative Perforated Steel Plate Shear Wall System with FRP Edge Reinforcement, Accepted for the 6th Intl. Symp. on Steel Structures, Korea.

Astaneh-Asl, A., 2002. Seismic Behavior and Design of Composite Steel Plate Shear Walls, Steel Tips Report, Structural Steel Educational Council.

Bambach, M.R., M. Elchalakani, and X.L. Zhao, 2009. Composite Steel–CFRP SHS Tubes under Axial Impact, J. Composite Structures, 87: 282-292.

Berman, J.W. and M. Bruneau, 2005. Experimental Investigation of Light-Gauge Steel Plate Shear Walls, J. Structural Engineering ASCE, 131(2): 259-267.

Driver, R.G., G.L. Kulak, D.J.L. Kennedy and A.E. Elwi, 1997. Seismic Behavior of Steel Plate Shear Walls, Struct. Eng. Rep. No. 215, Dept. of Civil Eng., Univ of Alberta, Edmonton, Alberta, Canada.

El-Damatty, A.A. and M. Abushagur, 2003. Testing and Modeling of Shear and Peel Behaviour for Bonded Steel/FRP Connections, J. Thin-Walled Structures, 41(11): 987-1003.

Harries, K.A., A.J. Peck, and E.J. Abraham, 2009. Enhancing Stability of Structural Steel Sections Using FRP, J. Thin-Walled Structures, 47: 1092-1101.

Hatami, F. and A.R. Rahai, 2008. An Investigation of FRP Composite Steel Shear Walls (CSSW) under Cyclic Loading on Laboratory, 14th World Conf. on Earthquake Eng., China.

Lapczyk, I. and J.A. Hurtado, 2007. Progressive Damage Modeling in Fiber Reinforced Materials. J. Composites, Part 38: 2333-2341.

Photiou, N.K., L.C. Hollaway and M. Chryssanthopoulos, 2006. Strengthening of an Artificially Degraded Steel Beam Utilizing a Carbon/Glass Composite System. J. Constr. and Building Materials, 20(11–21).

Rahai, A.R. and M. Alipour Tabrizi, 2010. Behavior and Characteristics of Innovative Composite Plate Shear Walls, 12th East-Asian Pacific Conf. on Structural eng. EASEC12, Hongkong.

Roberts, T.M. and S. Sabouri-Ghomi, 1992. Hysteretic Characteristics of Unstiffened Perforated Steel Plate Shear Panels, Thin-Walled Struct., 14: 139-155.

Sabouri-Ghomi, S., C.E. Ventura and M.H.K. Kharrazi, 2005. Shear Analysis and Design of Ductile Steel Plate Walls, J. Structural Engineering ASCE, 6: 878-889.

Shaat, A. and A. Fam, 2006. Axial Loading Tests on CFRP-Retrofitted Short and Long HSS Steel Columns. Canadian Journal of Civil Engineering, 33(4): 458-70.

Tavakkolizadeh, M. and H. Saadatmanesh, 2003. Strengthening of Steel–Concrete Composite Girders Using Carbon Fibre Reinforced Polymer Sheets, J. Structural Engineering, ASCE, 129(1): 30-40.

Teng, J.G. and Y.M. Hu, 2007. Behavior of FRP-Jacketed Circular Steel Tubes and Cylindrical Shells under Axial Compression, J. Construction and Building Materials, 21: 827-838.

Vian, D., M. Bruneau, K.C. Tsai, and Y.C. Lin, 2009. Special Perforated Steel Plate Shear Walls with Reduced Beam Section Anchor Beams. I: Exparimental Investigation. J. Struct. Eng., 135(3): 211-220.

Vian, D., M. Bruneau and R. Purba, 2009. Special Perforated Steel Plate Shear Walls with Reduced Beam Section Anchor Beams. II: Analysis and Design Recommendations. J. Struct Eng., 135(3): 221-228.

Xia, S.H. and J.G. Teng, 2005. Behavior of FRP-to-Steel Bonded Joints, Proc. Intl. Symposium on Bond Behavior of FRP in Structures, pp: 411-418.

Zhao, X.L. and L. Zhang, 2007. State-Of-The-Art Review On FRP Strengthened Steel Structures, J. Engineering Structures, 22: 1808-1823.